Advanced Materials

ADVANCED MATERIALS
www.advmat.de

RESEARCH ARTICLE

The Intersecting Physical Mechanisms That Regulate Cell Viability in 3D Synthetic Hydrogels

Nathan R. Richbourg[1,2,3,4] | Akaansha Rampal[1] | Adrian Lorenzana[1] | Juan F. Flechas-Beltran[2] | Shelly R. Peyton[1,2]

[1]The University of Massachusetts at Amherst, Amherst, Massachusetts, USA | [2]Tufts University, Medford, Massachusetts, USA | [3]FAMU-FSU College of Engineering, Tallahassee, Florida, USA | [4]Florida State University, Tallahassee, Florida, USA

Correspondence: Nathan R. Richbourg (nrichbourg@eng.famu.fsu.edu) | Shelly R. Peyton (shelly.peyton@tufts.edu)

Received: 27 October 2025 | **Revised:** 18 December 2025 | **Accepted:** 6 February 2026

Keywords: confinement | extracellular matrix | hydrogel design | poly(ethylene glycol) | transport

ABSTRACT

Hydrogels restrict protein transport to different extents, with nanoporous synthetic polymer networks providing far less protein permeability compared to microporous biopolymer networks. To evaluate whether reduced permeability was a driving factor in reduced cell viability in synthetic hydrogels, we compared poly(ethylene glycol) vinyl sulfone (PEG-VS) hydrogels with Matrigel to quantify the influences of modulus, transport, and confinement on encapsulated cells. We observed extensive reductions in cell viability when encapsulated in PEG-VS gels compared to Matrigel. In transwell experiments that decouple hydrogel-restricted serum from cell-gel adhesion, serum restriction reduced cell viability, matching the cell viability observed in 3D cultures. Our unique combination of 2D and 3D hydrogel-based cell cultures provides a framework for investigating the intersecting effects of the cell microenvironment's properties on cell viability. This work demonstrates that biomaterial-restricted protein transport is a critical design consideration when using synthetic 3D cell culture hydrogels.

1 | Introduction

By capturing some of the physical and biochemical properties of a cell's native extracellular matrix, hydrogel biomaterials provide key signals to gel-encapsulated cells [1]. Biopolymer-based hydrogels provide adhesive and structural cues comparable to native tissue, whereas synthetic polymer-based hydrogels can decouple network structure from cell adhesion and degradability [2]. The modularity of multi-arm poly(ethylene glycol) (PEG)-based hydrogels provides a unique opportunity to precisely modify a cell's 3D microenvironment [3, 4].

In 3D synthetic hydrogels, solute transport and modulus are usually inversely coupled [2, 5–7]. Therefore, precise characterization is needed to evaluate whether encapsulated cells are responding to the modulus of the gel or gel-restricted molecular transport when the network structure is altered [5]. Further confounding this story, some argue that confinement can alter cell behavior via mechanisms distinct from adhesion-dependent mechanosensing pathways. Early growth response protein 1 (EGR1) responds to stiffness differences in 3D encapsulation and not to the presence of integrin-binding sites, suppressing neurogenesis in stiffer substrates [8]. Critically, these competing influences on encapsulated cells suggest a need for more careful assessment of cell-environment interactions in 3D synthetic hydrogels. Restricted solute transport and cell confinement may explain why cells that proliferate to a greater extent on stiffer 2D substrates proliferate more slowly in stiffer 3D hydrogels [9].

Here, we used PEG-vinyl sulfone hydrogels to encapsulate cells in 3D microenvironments to specifically probe this question. We present here a new method of transport assessment, using hydrogels as membranes to restrict cell access to serum proteins, thereby independently tuning mechanical cues and solute

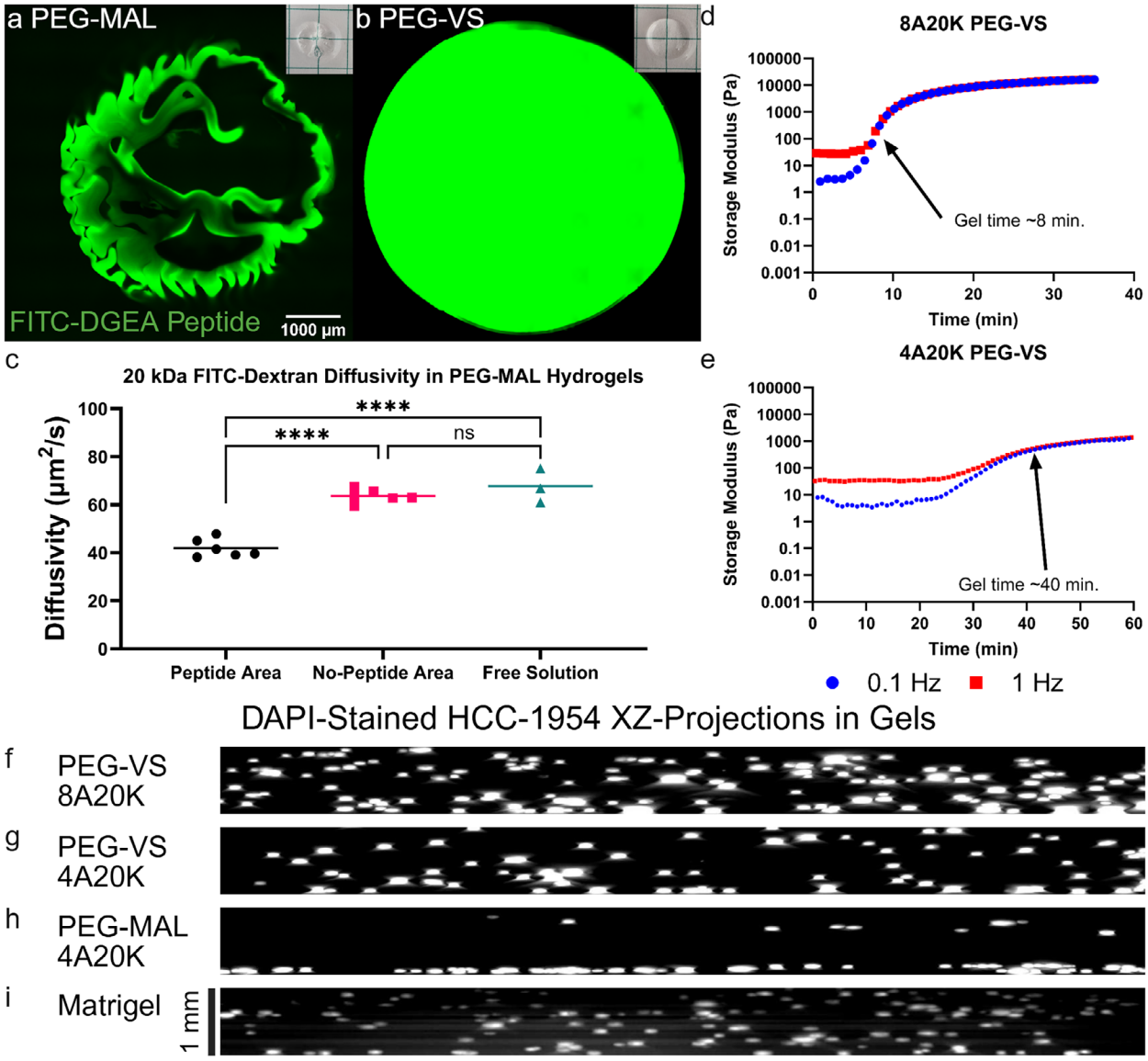

FIGURE 1 | Delayed gelation facilitates peptide and cell homogeneity in PEG-VS hydrogels. (a,b) Fluorescent peptide distribution in PEG-MAL hydrogels (a) and (b) PEG-VS hydrogels. Insets show hydrogel shape. (c) 20 kDa FITC-dextran diffusivity in peptide-containing and no-peptide regions of a PEG-MAL hydrogel (n = 6) compared to free solution diffusivity (n = 3). The line represents the mean, and symbols are individual values. Statistical significance was determined by one-way ANOVA with Tukey's multiple comparison test: ****$p < 0.0001$, ns, not significant. Peptide regions were located via a rhodamine-tagged peptide. (d,e) Gelation times for 8-arm, 20 kDa and 4-arm, 20 kDa PEG-VS hydrogel formulations determined by the Winter-Chambon criterion. (f–i) HCC-1954 cell distribution xz-projections in PEG-VS gels, PEG-MAL gels, and Matrigel. Full gel formulations in Table ST1.

transport. Integrin-binding and protease-degradable peptides were incorporated at varying concentrations, using structural hydrogel design to mitigate changes to hydrogel physical properties. These intersecting culture conditions revealed the substantial contributions of hydrogel-restricted solute transport and cellular confinement on cell viability in 3D synthetic hydrogels.

2 | Results

2.1 | Homogeneous and Tunable PEG-VS Hydrogels for 3D Cell Encapsulation

PEG hydrogels that use a maleimide terminal group (PEG-Mal) support protease-cleavable crosslinking and the incorporation of integrin-binding peptides to facilitate cell adhesion and migration through otherwise non-adhesive and nanoporous environments [10–12]. However, the well-documented kinetics of the maleimide-thiol reaction in aqueous environments require non-physiological or cytotoxic conditions to delay gelation enough to encapsulate cells in a homogeneous fashion [13, 14].

PEG-vinyl sulfone (PEG-VS) hydrogels form gels more slowly than PEG-Mal hydrogels, producing a more homogeneous hydrogel in both peptide and cell distributions. We confirmed this difference with fluorescently tagged peptides, which were heterogeneously distributed in PEG-Mal hydrogels (Figure 1a) and homogeneously distributed in PEG-VS hydrogels (Figure 1b). Furthermore, fluorescence recovery after photobleaching (FRAP)

experiments on 20 kDa FITC-dextran diffusion within the PEG-Mal hydrogels revealed a significant difference between the diffusion coefficients of the dextran in solution and in the high-peptide areas of the hydrogels, but no significant difference between solution and the no-peptide areas of the hydrogel (Figure 1c). These differences indicate that the no-peptide areas are in a liquid state. We attribute heterogeneous gelation to the rapid reaction of PEG-Mal and thiols at the surfaces where the two precursor solutions first came into contact, resulting in a poorly mixed, heterogeneous gel.

PEG-VS hydrogels prepared using 50 mM HEPES solution at pH 7.4 gelled in eight to 40 min (Figure 1d,e). Due to the slowed gelation of PEG-VS hydrogels, encapsulated cells were distributed throughout the gels, whereas cells were trapped at the top or bottom of the PEG-Mal gels (Figure 1f–i). Together, these results indicate that PEG-VS hydrogels can homogeneously encapsulate cells in a structurally homogeneous 3D environment under physiological conditions.

2.2 | pH is the Primary Determinant of PEG-VS Gelation With Complex Peptide Mixtures

To demonstrate the tunability of the PEG-VS hydrogels, we broadly investigated gelation conditions that supported the incorporation of integrin-binding and protease-cleavable peptides. 275 unique PEG-VS hydrogel formulations were attempted, and 182 formulations produced swellable gels. Because incorporating peptides caused gelation failure in a concentration- and pH-dependent manner (Gelation Table ST1), we assessed the contributions of gel precursor solutions to final pH. PEG-VS and PEG-dithiol negligibly affected the solution pH, but peptides greatly reduced pH (Figure 2a). We countered their pH reduction by increasing the initial pH of the HEPES solution (Figure 2b). Regardless of peptide presence, final solution pH values below 7.1 reliably failed gelation, indicating that the peptide-dependent gelation failures were due to decreasing the pH to the point that the vinyl sulfone-thiol reaction was unfavorable [15]. Even with varying peptide combinations, an initial solution pH of 7.8 consistently supported gelation and a final pH near 7.4, suitable for cell culture (Figure 2c).

2.3 | Adhesion and Degradation Drive Early Viability for Encapsulated Cells

Because cells are sensitive to the stiffness of their local microenvironment [16], we characterized the shear moduli of PEG-VS hydrogel formulations and Matrigel. We designed hydrogels with equivalent network structure parameters [2] such that stoichiometrically unsaturated and peptide-containing hydrogels had equivalent shear moduli (Figure 3a,b). 4-arm, 10 kDa (4A10K) and 8-arm, 20 kDa (8A20K) PEG-VS gels were much stiffer than their PEG-Mal counterparts due to increased network homogeneity [10, 11]. 4-arm, 20 kDa (4A20K) PEG-VS gels were comparable to the Matrigel moduli.

HCC-1954 breast cancer cells grew exponentially (measured by ATP activity assay) when encapsulated in Matrigel over 7 days and rapidly died within PEG-VS gels (Figure 3c). We initially hypothesized that the difference in cell growth was due to a low concentration of integrin-binding sites in the PEG gel, particularly in comparison to Matrigel [17]. Because further increasing the RGD concentration in 4A20K gels caused gelation to fail, half-crosslinked 8A20K (8A20K-HX) gels were synthesized to support RGD incorporation up to 10 mM without

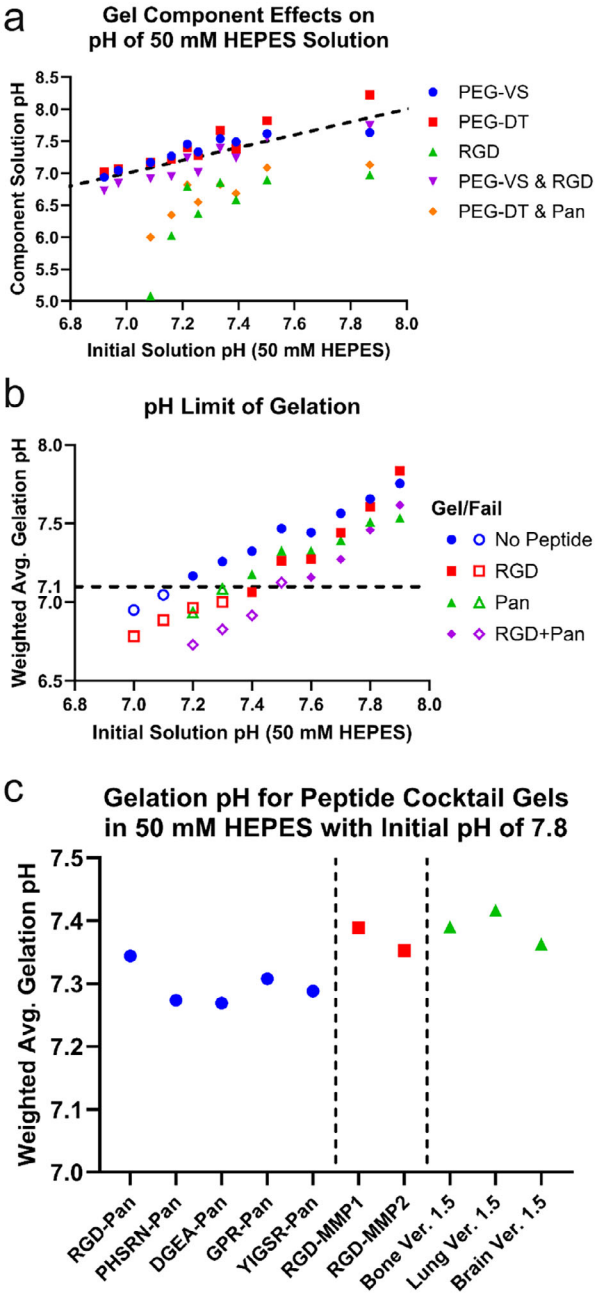

FIGURE 2 | Gelation depends on network structure parameters, solution pH, and peptides. (a) The effects of pre-gel components on solution pH at concentrations used to make a 10% 4A20K PEG-VS hydrogel with 2 mM RGD and 25% degradable crosslinks. The dotted line represents the equivalent pH for the initial solution and the solution with pre-gel components. (b) Gelation pH for gels containing different peptide combinations. The dotted line represents the apparent pH cutoff for gelation. (c) Gelation pH values for varying peptides incorporated in gels using a pH 7.8 initial HEPES solution. Dotted lines separate groups of formulations. Full gel formulations in Table ST1.

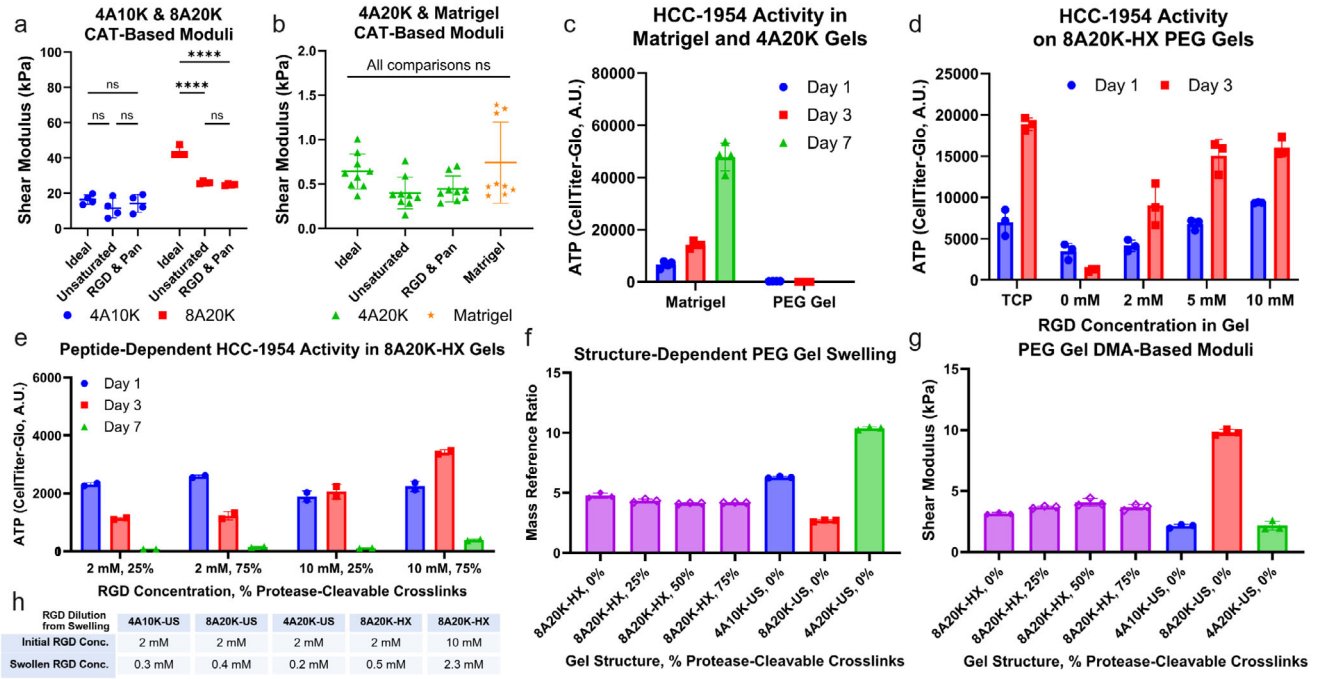

FIGURE 3 | Cell-gel adhesion supports short-term survival in encapsulation. (a,b) Shear moduli of multi-arm PEG hydrogels and Matrigel (a, n = 4, b, n = 9). Statistical significance was determined by one-way ANOVA with Tukey's multiple comparisons test: ****$p < 0.0001$, ns, not significant. (c) HCC-1954 ATP activity when encapsulated in Matrigel or a 4A20K PEG hydrogel (n = 4). (d) HCC-1954 ATP activity on 2D PEG hydrogel substrates with varying RGD concentrations (n = 3). (e) Cell ATP activity when encapsulated in hydrogels with combinations of RGD concentration and protease degradability (n = 2). (f–h) Structure-dependent gel swelling (f) and moduli (g), and swelling contributes to (h) RGD dilution. All values represent the mean ± s.d. Full gel formulations in Table ST1.

affecting network structure. For 4A20K gels that were made with 2 mM RGD, swelling to equilibrium diluted the final RGD concentrations experienced by cells to 0.3 mM (Figure 3f,h). For 8A20K-HX gels prepared with 10 mM RGD, the swelling was diluted to 2.3 mM at equilibrium. The need for the higher RGD concentration is consistent with prior reports that 2–4 mM RGD is needed for cell viability [18, 19]. Although increasing initial RGD concentration to 10 mM increased cell adhesion and growth over 3 days on 2D gel substrates to levels comparable to tissue culture polystyrene (TCPS; Figure 3d), cells were still unable to grow over 7 days in 3D encapsulation culture (Figure 3e).

We then hypothesized that the cells in 3D were growth-limited by their largely non-degradable environment. We therefore increased the degradable fraction of crosslinks, yielding gels with equivalent swelling and moduli at different degradable fractions (Figure 3f,g). However, increasing the fraction of protease-degradable crosslinks from 25% to 75% still did not increase growth over 7 days (Figure 3e). The combination of 10 mM RGD and 75% degradability yielded an increase in ATP activity on day 3, but still did not support growth from day 3 to day 7. Noting that others have achieved cell growth in 100% protease-degradable, low-polymer concentration PEG-VS hydrogels [20], we chose instead to continue investigating whether sustained cell growth can be achieved in a hydrogel that is not fully degradable, as this would keep degradability an independently controllable design parameter.

2.4 | Solute Transport Regulates Survival of Cells Encapsulated in Nanoporous Synthetic Hydrogels

To specifically determine whether transport limitations were responsible for the lack of cell viability at these extended time points, we devised an approach to separate the effects of modulus and crosslinking from transport restriction (Figure 4a). We first cultured cells on a hydrogel substrate, providing adhesion signaling, and/or separated from serum by a gel-coated transwell to regulate solute transport. Serum-containing and serum-free media on TCPS provided positive and negative controls for serum-dependent cell growth. Serum-free culture reduced the growth of both HCC-1954 breast cancer cells and HS-5 bone marrow stromal fibroblasts (Figure 4b,d). HCC-1954s were more sensitive to serum deprivation than HS-5s, with a net decrease in HCC-1954 ATP activity over 7 days in the serum-free conditions. These serum-dependent growth trends were maintained in transwell experiments. Cells in the transwell-only condition grew slowly despite the reduced serum concentration. 1x serum within the transwell yielded an average serum concentration across the transwell equal to 20% of full-serum media. In a supplemental study, 5x serum in the transwell matched serum-containing culture growth (Figure S1b). Hydrogel-restricted serum yielded the same no-growth trend observed in serum-free culture (even with 5x serum). The hydrogel coatings in this experiment were 20 μL in volume, yielding a coating in the 24-well plate transwells less than 1 mm thick. All serum transport conditions were repeated with a 10 mM RGD gel substrate below the cells to evaluate whether cell

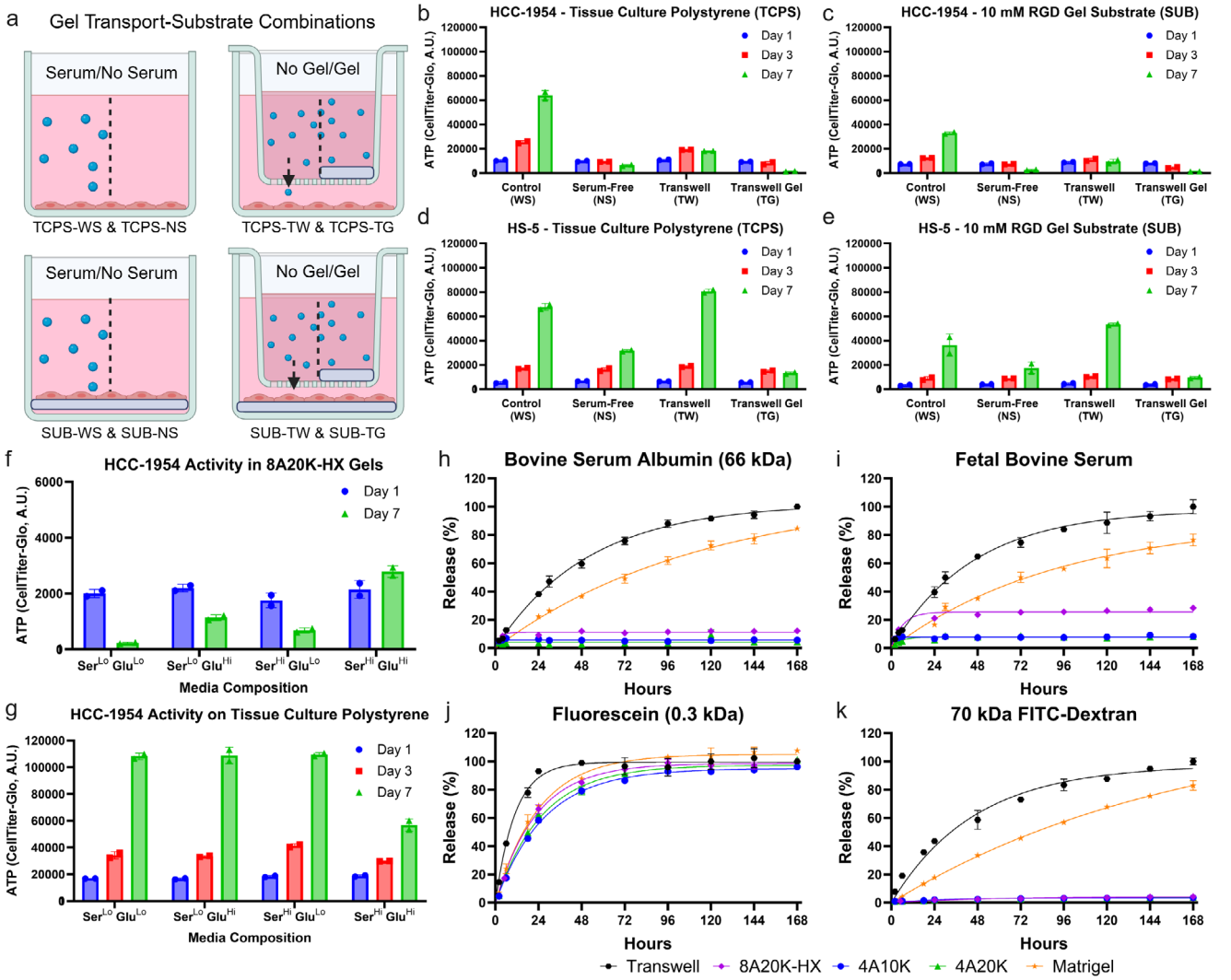

FIGURE 4 | Hydrogel-restricted serum access regulates cell ATP activity. (a) Schematic summary of 2D cell-gel adhesion and transport conditions used in b-e. b-e, Cell ATP activity for HCC-1954s (b,c) and HS-5s (d,e) on TCPS (b,d) and on a 10 mM RGD gel substrate (c,e). (f,g) High serum (20% vs 10%) and high glucose (4.5 g/L vs 2 g/L) media were tested for cells in 8A20K-HX gels (f) and on TCPS (g). (h–k) Protein transport (h,i) and fluorescent solute transport (j,k) were independently measured through transwells with varying gel coatings. n = 2 for all experiments. In bar charts (b–g), values represent the mean ± s.d. with symbols for individual results. In release plots (h–k), symbols represent mean ± s.d. and the lines represent the best fit of a one-phase association model. Full gel formulations in Table ST1.

-gel adhesion affected serum dependence. The serum-dependent trends were repeated with reduced total ATP activity on all gel substrates (Figure 4c,e), attributed to reduced cell growth capability on a soft gel substrate with specific cell adhesion sites compared to broadly adhesive TCPS. Together, these results indicate that HCC-1954s are more sensitive to serum deprivation than HS-5s, but serum transport restriction by hydrogels deprives cells of serum proteins that support cell growth.

To promote gradient-driven transport into hydrogels, we increased the concentrations of serum and glucose in the media. For gel-encapsulated HCC-1954s, the combination of increased serum and glucose increased the ATP from day 1 to day 7 (Figure 4f). While the change does not indicate substantial cell growth, it was a marked improvement from the outright cell death by day 7 in all other PEG-VS encapsulation cases. On 2D TCPS, the high-serum, high-glucose formulation slightly reduced cell growth (Figure 4g). Although the reason for this is unclear (it may be associated with cell maladaptation to large changes in media components [21]), it further distinguishes the improved growth in the case of 3D encapsulation.

Characterization of solute transport through transwells and gel-coated transwells indicates that small solutes pass through the PEG gels, but larger solutes do not (Figure 4h–k; Figure S2). Solute transport through Matrigel is comparable to transport through uncoated transwells, therefore providing a plausible explanation for why cells readily grow within Matrigel but not PEG gels. Together, these results indicate that cell growth is highly sensitive to solute transport, and reduced cell viability in 3D PEG gel encapsulation might be due to restricted solute transport.

2.5 | Cell Confinement in PEG Gels Restricts Growth Across Cell Types

On 2D surfaces, cells sense and respond to modulus using traction forces. However, in 3D nanoporous matrices, increases in modulus also allow for compressive force. This added cue of compression or confinement can mean that cells are sensitive to far smaller ranges of moduli in 3D compared to 2D when integrin-binding concentrations are comparable [8]. This mechanosensing in 3D appears to be more cortical actin- than microtubule-dependent. Signaling from total confinement reduces cell growth [8]. With our modular hydrogels, we investigated the contribution of confinement to cell viability in 3D encapsulation culture. In addition to ATP assays, live/dead-stained cells in 3D cultures were counted at days 1, 3, and 7 (Figure 5a–d). Across multiple cell types (HCC-1954s, HS-5s, MDA-MB-231 breast cancer cells, and NIH-3T3 mouse fibroblasts), live cells consistently decreased, dead cells increased, and total cells remained nearly unchanged over 7 days.

To determine which physical property was the primary driver for the observed growth restriction, we postulated that cells toward the top surface of the hydrogels, with a shorter diffusion distance to serum- and glucose-rich media, would grow more than cells in other regions if solute transport was the primary factor. Conversely, cells within one cell diameter from the TCPS surface would experience a relatively stiff environment and grow more if stiffness were the primary factor. However, the trends for live and total cell counts in each region over time were consistent with the overall values (Figure 5e; Figure S3a), suggesting that confinement may be a primary environmental regulator of cell viability in 3D PEG-VS hydrogels. This secondary data analysis is presented as a supporting argument that warrants further validation and mechanistic investigation.

The live cell counting results diverge from the ATP activity assay results (Figure 5f), which show increases in ATP on day 3 for HCC-1954s, MDA-MB-231s, and HS-5s. These bulk assays may suggest that, despite many cells dying, the remaining cells have increased their ATP production. It could also be a methodological error arising from growing cells forming clusters that are indistinguishable as individual cells in the live/dead assay and 3D Imaris reconstruction used to count the cells. Notably, the divergence was not observed in 2D cultures, regardless of serum and transwell conditions (Figure S4). Furthermore, the number of HCC-1954 cells alive in 3D on day 7 was higher in the high-glucose, high-serum media than in the other media compositions (Figure S5h), which is a consistent trend with the ATP results. These data suggest that solute transport restriction remains a contributor to cell viability in 3D encapsulation, but it may be secondary to confinement.

Cell motility in the PEG-VS gels was nearly completely restricted, irrespective of both polymer weight percent and concentration of protease-degradable crosslinks, further promoting confinement as a driver of cell phenotype in these synthetic environments (Figure 5g,h). Cells in PEG-VS gels had significantly lower displacements and path straightness than Matrigel, suggesting an inability to degrade their surroundings and migrate. This was true even in 6% polymer volume fraction PEG-VS hydrogels, suggesting these gels were still above a network density threshold restricting cell movement (Figure S6 further characterizes cells encapsulated in 6% PEG-VS hydrogels). Although the switch from 25% degradability to 75% was critical for improving short-term cell ATP activity (Figure 3e), the negligible effect on cell motility indicates that the molecular network of a PEG hydrogel may be too densely interconnected for MMP-mediated degradation to enable cell motility, at least for the combinations of polymer volume fractions and degradable crosslink fractions studied here [22, 23]. This could be because the mesh radius of the partially degraded PEG network is still orders of magnitude smaller than the radius of a cell, even when each protease-cleavable peptide is cleaved within a 75% degradable gel. This would mean that even if each protease-cleavable crosslink is cleaved, cells would be unable to move through the hydrogel due to the remaining non-degradable crosslinks. This interpretation is supported by the fact that 8A20K-HX gels with 75% degradable crosslinks did not fully dissolve after 5 days of incubation in a 0.01x trypsin solution (Figure S7j). Values approaching 100% degradability may be more impactful on cell viability than the change from 25% to 75% degradable.

3 | Discussion

We present a new method to evaluate the independent roles of modulus, transport, and confinement on viability in 3D synthetic PEG gels. As predicted by the Swollen Polymer Network model [7, 24–26], homogeneous nanoporous hydrogels dramatically restricted the transport of serum proteins, which are critical for cell metabolism [27]. By using a hydrogel-coated transwell separating cells from serum, we demonstrated that the serum restriction due to a thin PEG-VS hydrogel is sufficient to stop proliferation in HCC-1954 breast cancer cells. The serum dependence in 2D is strongly implicated as a contributing factor to limited cell proliferation in 3D. This approach, using combinations of a cell-adhesive hydrogel substrate and a protein-restricting hydrogel, provides an avenue for independently evaluating the competing physical signals a cell receives in 3D synthetic hydrogels. Whereas large solute transport clearly plays a governing role in the viability of cells in 3D PEG hydrogels, experiments focused on the mechanical properties of hydrogels have largely driven the collective understanding of cell responses to 3D encapsulation culture [16, 28]. This work aimed to highlight this overlooked physical factor in cell-gel interactions.

Given that PEG-Mal gels have been used by us and others to successfully encapsulate cells at higher PVFs, we initially compared using PEG-Mal hydrogels, photoinitiated PEG-norbornene hydrogels (Figure S8) [29–32], PEG-methylsulfone [33], and triethanolamine-catalyzed PEG-VS gelation [34, 35], but none were suitable for our goals. The PEG-Mal kinetics formed heterogeneous gels, PEG-methylsulfone was prohibitively challenging to synthesize, and the photoinitiation and triethanolamine approaches introduced cytotoxic radicals. However, each of these gelation approaches provides specific advantages and remains suitable for other applications, such as when cells can be seeded onto gel substrates or pre-formed microgel aggregates [36].

Prior reports of cell encapsulation in HEPES-catalyzed PEG-VS hydrogels used 8-arm, 20 kDa PEG-VS at approximately 50% crosslinking in solutions of 10x PBS and 1 M HEPES at pH

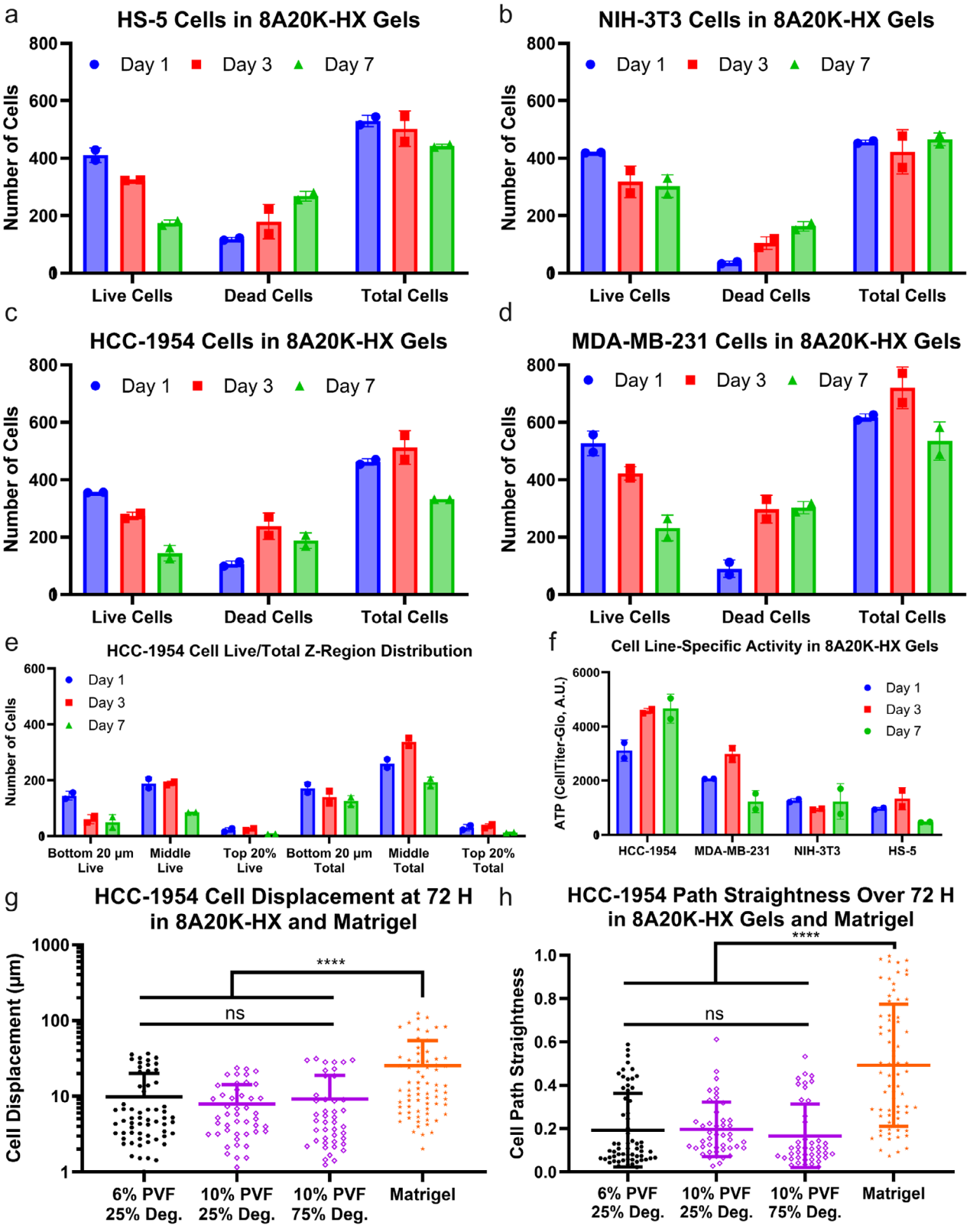

FIGURE 5 | Confinement contributes to restricted cell growth and motility in PEG gels. (a–d) Counts of live, dead, and total cells in PEG-VS gels over 7 days. Cell types are HS-5 (a), NIH-3T3 (b), HCC-1954 (c), and MDA-MB-231 (d). (e) Vertically binned HCC-1954 cell distributions of live and total cells. (f) ATP activity of the four cell lines over time. (g,h) Displacement (g) and path straightness (h) of HCC-1954 cells in varying PEG gels and Matrigel over 3 days. For (a–f) n = 2. For g,h, n = 44–70. Statistical significance was determined by one-way ANOVA with Tukey's multiple comparisons test: ****$p < 0.0001$, ns, not significant. Values represent the mean ± s.d. with symbols for individual results. Full gel formulations in Table ST1.

7.8 or 8.2 [20, 37]. The highly buffered solutions may be what enabled them to form gels at 3–7 wt.% macromer, whereas our formulations were unable to gel below 6% v/v. Cells were able to rapidly grow and even escape their hydrogel formulations, which were made with 100% protease-degradable crosslinks. This contrasts with our consistent cell death, suggesting that our partially degradable, highly crosslinked gels excessively confine encapsulated cells, and crosslinking degradability near 100% may be necessary for cell growth in PEG-VS hydrogels [22]. Critically, gel degradation increases the frequency of chain-end defects, simultaneously changing stiffness, swelling, and solute transport (Figure S7) [7]. We found methods for characterizing the effects of gel degradation underreported, so protocols for measuring gel degradation over time and associated changes to stiffness and transport are presented in the supplementary materials. Intentional design for hydrogel degradation is an important consideration for current and future hydrogel applications [38–40]. A study using 3–5 wt.% 8A20K PEG-norbornene found that endothelial cells were unable to grow above 4 wt.% or 45% crosslinking with degradable crosslinks or in the 3%, 35%-crosslinked condition with non-degradable crosslinks [41]. These data corroborate our conclusion that cell proliferation is limited by confinement in 3D PEG gels with relatively high polymer concentrations and a substantial fraction of nondegradable crosslinks.

The portals of a well-crosslinked PEG-VS hydrogel, even at a stoichiometric crosslinking ratio of 50% for the 8A20K-HX formulations, have radii on the order of 10 nm [5, 24]. This mesh radius is far less than what would be found in a heterogeneously crosslinked PEG-MAL hydrogel, or a PEG-VS hydrogel with the polymer concentration below the polymer overlap concentration, which would also form a heterogeneous gel. Matrigel's network structure, which includes heterogeneous crosslinking and more rigid, fiber-like protein structures, has portal radii on the order of 10 mm. These spacings are dependent on the hydrated state of the materials and cannot be accurately assessed using typical microscopy techniques [42], but they can be inferred from solute and cell transport through the materials. The nanometer-scale portal size of PEG-VS hydrogels supports greatly restricted transport of nanometer-scale proteins but presents an impassable wall to micrometer-scale cells. In principle, even at 75% degradable crosslinks, a cell would not be able to degrade a PEG-VS network enough to reliably create a cell-sized space for movement through the network, especially at rates comparable to Matrigel, which is inherently cell-permissible as well as cell-degradable. This difference in network scaling supports our earlier argument that a PEG-VS hydrogel would likely have to be nearly 100% degradable and/or formulated heterogeneously below the polymer crossover concentration to enable encapsulated cell motility. Further experimental design and characterization using these principles could identify whether specific solute diffusion coefficients and/or degradable crosslink fractions could predict cell viability and motility. The scope of this work was to define the overlapping environmental limitations to cell culture in PEG-VS hydrogels.

Because we were specifically interested in the role of transport, modulus, and confinement on cell viability, we limited our phenotypic assays to ATP activity and the Live/Dead assay kit. We acknowledge that these methods provide limited biomolecular insight into cell behaviors, so this study presents a preliminary application of these cell-environment control methods. However, our approach, which emphasizes solute transport effects, could be extended to mechanisms of cell death, senescence, and even motility, as we present in Figure 5 [9]. Existing biomolecular tools used to probe cell characteristics, such as the live fluorescent reporter of cell cycle phase FUCCI [43], can synergize with transport-controlled culture [44]. Further studies could identify molecular targets for how solute transport and confinement each contribute to encapsulated cell behaviors, leading to routes to overcome these barriers to cell viability in synthetic hydrogels. Evaluating specific cell interactions with bioactive peptides in hydrogels with controlled physical properties is a growing area of study, and the hydrogels developed here further support those investigations [4, 10, 45].

4 | Methods

All reagents and solvents were purchased from MilliporeSigma unless otherwise specified and used without further purification. All components containing PEG were purchased through JenKem. All peptides were purchased from GenScript.

4.1 | PEG-VS Hydrogel Gelation

PEG-vinyl sulfone (PEG-VS) hydrogel gelation was adapted from prior protocols and optimized using the modular hydrogel design calculator developed for this study [10–12, 37]. The modular hydrogel design calculator is available in the DOI links in the Supplemental Materials. Based on the desired volume and structural parameters of the desired gel, the modular hydrogel calculator provides a reproducible step-by-step recipe for creating a target gel formulation, including changes to the structure of the main multi-arm PEG macromolecule (number of arms and molecular weight), the length of the crosslinking PEG-dithiol, the initial polymer volume fraction, the crosslinking stoichiometric ratio, and the incorporation of integrin-binding and crosslinking peptides or peptide cocktails as desired. Each PEG-VS hydrogel formulation tested for this study, including those that failed to gel, is recorded in the gelation spreadsheet (linked in the Supplemental Materials). For a typical gelation, four-arm, 20 kDa PEG-VS was dissolved in 50 mM HEPES at pH 7.8 and then mixed with the integrin-binding peptide G**RGD**SP**C**G, also suspended in 50 mM pH 7.8 HEPES. At the same time, 1.5 kDa PEG-dithiol was mixed with protease-cleavable dithiol peptide G**C**RD**GPQGIWGQ**DR**C**G, both in HEPES. These two mixed solutions were combined to yield the final gelation solution, resulting in an RGD concentration of 2 mM, a total polymer volume fraction of 10%, 25% of the crosslinking being protease-cleavable, and stoichiometric equivalence between total thiols and vinyl sulfone groups available. Gels were typically formed in 10 or 20 μL volumes within 24-well plates and completed gelation within 40 min either at room temperature or 37°C.

4.2 | PEG-Maleimide Hydrogel Gelation

PEG-maleimide (PEG-Mal) hydrogels were made as previously described with structural modifications to compare their

properties to PEG-vinyl sulfone hydrogels [10–12]. Briefly, multi-arm PEG-Mal (typically four-arm, 20 kDa) was dissolved in PBS (concentrations 0.1–10X, pH 6–8 for varying experiments) and mixed with a solution of PEG-dithiol (typically 1 kDa, Jenkem, USA) in PBS at stoichiometric maleimide-thiol ratios to form a gel within a minute of mixing. Alternatively, PEG-dithiols were partially substituted by the dithiol-terminated protease-cleavable peptide sequence G**C**RD**GPQGIWGQ**DR**C**G, and/or the thiol-terminated integrin-binding peptide G**RGD**SP**C**G was added to the PEG-Mal precursor solution at defined concentrations. Adjustments were made to crosslinking stoichiometry to negate competition between integrin-binding peptides and crosslinking components for maleimide groups.

4.3 | PEG-Norbornene Hydrogel Gelation

PEG-Norbornene hydrogels made using 8-arm, 20 kDa PEG-norbornene precursor macromers and 1.0 kDa PEG-dithiol as crosslinkers in a 1xPBS solution. Initial gelation studies explored LAP concentrations of 0.1, 1, and 10 mM, a 365 nm mercury lamp UV source or a 405 nm LED (light intensities held at 3 mW/cm^2), exposure times of 10 s, 1, or 10 min, and polymer volume fractions of 2%, 5%, and 10%, all at stoichiometric crosslinking.

4.4 | Matrigel Gelation

Matrigel (Corning) at as-purchased concentrations of 8–10 mg/mL was gelled without dilution by incubating 10 or 20 µL volumes at 37°C for 30 min.

4.5 | Gelation Characterization and Micro-pH Measurements

Gelation was evaluated by adding 1 mL of PBS to a 20 µL gel in a 24-well plate well after 40 min of gelation unless otherwise specified. If there was no visibly intact gel after the PBS was removed or if most of the gel was removed, the gelation failed. To evaluate gelation pH conditions, the pH of gel precursor solutions was measured using a fiber optic pH probe (pH-1 micro, PreSens Precision Sensing). A volume-weighted average of the final precursor solutions was used to estimate the pH of the gel since the fragile pH probes were not intended to pierce a gel.

4.6 | Rheological Gelation Time Characterization

Gelation times, storage moduli (G'), and $\tan(\delta)$ of gel components were determined on a Kinexus Pro parallel plate rheometer (Netzsch). Immediately before rheological measurements, gel precursor solutions were pipetted into a 1.5 mm microcentrifuge tube and vortexed for 5 s. Measurements were run on a 20 mm plate with a 1 mm gap at 0.1% strain. Measurements were taken at 0.1 and 1 rad s^{-1}. The gel point was defined using the Winter-Chambon criterion, for which the time of gelation is defined as the point at which the storage modulus becomes frequency-independent at small frequencies [46, 47]. Rheological experiments were analyzed using IRIS Rheo-Hub (IRIS Development) [48].

4.7 | Hydrogel Shear Modulus Measurements

Initial hydrogel shear modulus measurements were made using a contact adhesion tester (CAT) developed by the Crosby lab at the University of Massachusetts [49]. Briefly, a 4 mM glass hemispherical probe was indented up to 20% of the gel's initial height into an equilibrium-swollen 20 µL hydrogel hemisphere on a glass slide. Force was measured via deflection of a calibrated cantilever supporting the glass probe. The force-displacement relationship was interpreted using the Hertz model as previously described to yield a characteristic shear modulus for the hydrogel [5, 50].

Later, hydrogel shear modulus measurements were made using a dynamic mechanical analyzer (DMA; TA Discovery DMA850) at Tufts University. A flat metal surface was used to compress equilibrium-swollen 20 µL gels on plastic coverslips up to 20%, and the force-displacement relationship was also interpreted using the Hertz model [50].

4.8 | Solute Transport Measurements

Fluorescence recovery after photobleaching (FRAP) was used as previously described as an initial characterization of the solute transport capacity of individual hydrogel formulations [24, 26]. Specifically, 20 µL hydrogels were synthesized and then swollen in a 10 µM solution of a specific fluorescent solute in 1x phosphate-buffered saline (PBS). After 24 h of gel incubation with the solute, FRAP experiments were performed on the hydrogels using a Nikon A1R18 confocal scanning microscope (Nikon, UMass Light Microscopy Core Facility). Three samples were prepared for each pairing of gel formulation and solute, and each sample was used for three FRAP experiments. The fluorescent solutes used were fluorescein sodium salt, 20 kDa FITC-dextran, 70 kDa FITC-dextran, and 150 kDa FITC-dextran. FRAP analysis was performed as previously described using a high-throughput FRAP analysis script in MATLAB (Mathworks).

Transwell transport experiments were performed to assess solute transport through gels in a format comparable to cell encapsulation. Gels of either 100 or 20 µL were formed within transwell inserts (cellQART 24-Well Cell Culture Insert PET, 0.4 µm, Clear, Sterlitech), and the transwells were placed within wells containing PBS. A solution of PBS and the solute of interest (fluorescein, 20, 70, or 150 kDa FITC-dextran, bovine serum albumin (BSA), or FBS) was then placed within the transwell. Solute release into the outer well was observed over 7 days. An empty transwell was used as a control condition showing rapid transport. For fluorescent solutes, fluorescence in the wells with transwells removed was measured at each time point. For BSA and FBS, samples were taken from the lower wells and assessed for protein content using a microBCA assay (Thermo Fisher).

4.9 | Degradation and Swelling

Hydrogel swelling was measured using mass-based measurements. We have previously demonstrated that mass-based swelling ratios for hydrogels with well-defined polymer chemistry are comparable to volumetric swelling ratios [6]. The masses of

coverslips were measured, and 20 μL of hydrogels were formed on coverslips. Initial masses were measured after gelation was complete, and then the gels were swelled for 24 h in PBS. Swollen masses were measured, and the reported mass reference ratio is the swollen gel mass divided by the initial gel mass.

Swelling-based degradation studies were performed by taking swollen gels of known masses and incubating them in dilute trypsin (0.01x) or collagenase (0.001 mg/mL) solutions for up to 5 days, replacing the solution daily. Samples were carefully dried of excess solution each day and measured to track changes in mass over time.

Accelerated degradation experiments used 0.1x trypsin for 24 h, and resulting mass swelling or changes in mechanical or solute transport properties were measured as described above.

4.10 | Cell Culture

Cells from the HCC-1954 breast cancer cell line (ATCC) were expanded on tissue culture polystyrene (TCPS) in RPMI 1640 (Gibco) medium with L-glutamate, 10% fetal bovine serum (FBS), and 1% penicillin/streptomycin supplemented. Serum-free conditions used RPMI 1640 medium with L-glutamate and 1% pen/strep. HCC-1954 cells were used for experiments at passages 3–10. Generally, cells were lifted via trypsin treatment between passages and for aliquoting into experimental conditions.

The NIH-3T3 mouse fibroblast cell line (passage 5–12, ATCC), the human triple negative breast cancer MDA-MB-231 cell line (passage 30–40, ATCC), and the human bone marrow fibroblast-like HS-5 cell line (passage 3–10, ATCC) were each expanded in Dulbecco's minimum essential media (DMEM, Gibco) with 10 FBS and 1% pen/strep. Serum-free conditions used DMEM with 1% pen/strep.

4.11 | 2D Cell Culture Variant Conditions

For 2D cell culture experiments, cells were cultured in 24-well plates either directly on TCPS or on a thin, 20 μL layer of hydrogel. Media was either serum-containing, serum-free, or 1 mL of serum-free and a transwell with 200 μL of 10% serum-containing medium. Transwells were used with or without a 20 μL gel layer covering the bottom membrane. Cells were seeded at 5,000 cells/well for 2D culture experiments.

4.12 | 3D Cell Encapsulation

For 3D cell encapsulation experiments, 2 000 cells were encapsulated in 10 μL of gel and cultured in serum-containing or serum-free media after 40 min of gelation time in the incubator. For initial cell distribution experiments that do not use live/dead stains, cells were cultured for 24 h, then fixed, permeabilized, and stained with DAPI using standard protocols.

4.13 | Cell ATP Activity and Viability

To assess cell ATP activity and viability, live cells were first imaged using the fluorescent live/dead kit (calcein-AM and ethidium homodimer-1, Thermo Fisher) on a Zeiss Axiovert widefield fluorescence microscope for 2D and 3D cultures and on a Zeiss Axiovert spinning disc confocal microscope for 3D cultures. Cells were stained for microscopy following the manufacturer's protocols. Following microscopy, cell ATP activity was assessed using the CellTiter-Glo 2.0 assay (Promega), following the manufacturer's protocols [51]. Luminescence was read using a BioTek Synergy H1 plate reader (Agilent).

4.14 | Fluorescent Peptide Incorporation and Imaging

Fluorescent peptides were generated by reacting a fluorescent probe (fluorescein 5-isothiocyanate or rhodamine B isothiocyanate) with the terminal groups of the peptides. Fluorescent peptides were incorporated into hydrogels using the approach described above for gelation. Fluorescent gels were imaged after swelling using a Nikon A1R18 confocal scanning microscope (Nikon, UMass Light Microscopy Core Facility).

4.15 | Image Analysis and Quantification

Cell microscopy images were analyzed using Zeiss Zen and Imaris (Oxford Instruments). For 3D images, maximum orthogonal xz and xy projections were produced in Zen. Cell distributions, counting, and motility were analyzed using the spots and vantage tools in Imaris. Final figures were made using GraphPad Prism.

4.16 | Statistical Analysis

All statistical analysis was performed in GraphPad Prism using one-way ANOVA with Tukey's multiple comparisons test. Statistical significance comparisons were only assessed for groups with $n \geq 3$.

All cell activity, viability, and total cell count experiments were performed with $n = 2$ per group and were assessed for trends with respect to time and not for statistically significant differences between groups due to the low number of replicates. The quality of the results was cross-validated between the live/dead staining and the ATP assays to support robust conclusions despite the low replicate numbers (Figures S4 and S5). The low replicate numbers were chosen to reduce experimental costs while investigating several competing conditions within single experiments, therefore minimizing temporal and biological contributions to variability. Specifically, 24-well plates (selected for substantial cell counts per well and 24-well transwell inserts to be consistent with transwell transport experiments), which used outer wells as PBS-containing humidity buffers to minimize edge effects, yielded 8 usable wells per experiment. To compare four groups in a plate, two wells were used per group. Further replications were limited by the costs of materials, including the transwells, gel components, and stain and assay components. Trends observed using this approach are expected to be precisely reproducible, as can be observed in consistent values for control groups across multiple experiments (e.g., Figure 4b,g; Figure S1b,c control conditions).

4.17 | Detailed Protocols and Data Repository

All protocols for experiments in this study and related raw and processed data are available online via Figshare at the DOIs listed in the Supplemental Materials.

Acknowledgements

The authors thank Serena Birnbaum and Al Crosby for training on and use of their contact adhesion tester. Thanks also to James Chambers at the UMass IALS Light Microscopy Facility for training and use of the A1R18 microscope for FRAP experiments. Thanks to Laura Place at the Tufts University BME Department for training on the DMA. We thank Cole Haag, Ezekiel Eliamani, Emily Gong, Asher Baynes, Rebecca E Huber, Ninette Irakoze, Auggie Wirasaputra, and Tianna Edward for discussions and preliminary data collection relevant to this manuscript. We thank attendees of the 2023 Biomaterials and Tissue Engineering Gordon Research Conference for gel synthesis advice that helped to guide this study. During this project, N.R. was supported by the ODET NIH T32 program number 5T32EB016652-10 and NSF CMMI-2403731. AR was supported by NIH R01 CA273010. AL was supported by NIH U01 CA265709. JFFB was supported by NSF CMMI-2403731. SRP was supported by funding from Tufts University.

Conflicts of Interest

The authors declare no conflict of interest.

Data Availability Statement

The data that support the findings of this study are openly available in Figshare at https://doi.org/10.6084/m9.figshare.c.8040718.v1, reference number 8040718.

References

1. C. Ligorio and A. Mata, "Synthetic Extracellular Matrices With Function-encoding Peptides," *Nature Reviews Bioengineering* 1 (2023): 518–536, https://doi.org/10.1038/s44222-023-00055-3.

2. N. Richbourg, M. E. Wechsler, J. J. Rodriguez-Cruz, and N. A. Peppas, "Model-based Modular Hydrogel Design," *Nature Reviews Bioengineering* 2 (2024): 575–587, https://doi.org/10.1038/s44222-024-00167-4.

3. A. J. Garcia, "PEG–maleimide Hydrogels for Protein and Cell Delivery in Regenerative Medicine," *Annals of Biomedical Engineering* 42 (2014): 312–322, https://doi.org/10.1007/s10439-013-0870-y.

4. A. Y. Clark, K. E. Martin, J. R. García, et al., "Integrin-specific Hydrogels Modulate Transplanted human Bone Marrow-derived Mesenchymal Stem Cell Survival, Engraftment, and Reparative Activities," *Nature Communications* 11 (2020): 114, https://doi.org/10.1038/s41467-019-14000-9.

5. N. R. Richbourg and N. A. Peppas, "Structurally Decoupled Stiffness and Solute Transport in Multi-arm Poly(ethylene glycol) Hydrogels," *Biomaterials* 301 (2023): 122272, https://doi.org/10.1016/j.biomaterials.2023.122272.

6. N. R. Richbourg, M. Wancura, A. E. Gilchrist, et al., "Precise Control of Synthetic Hydrogel Network Structure via Linear, Independent Synthesis-swelling Relationships," *Science Advances* 7 (2021): abe3245, https://doi.org/10.1126/sciadv.abe3245.

7. N. R. Richbourg and N. A. Peppas, "The Swollen Polymer Network Hypothesis: Quantitative Models of Hydrogel Swelling, Stiffness, and Solute Transport," *Progress in Polymer Science* 105 (2020): 101243, https://doi.org/10.1016/j.progpolymsci.2020.101243.

8. J. Baek, P. A. Lopez, S. Lee, T.-S. Kim, S. Kumar, and D. V. Schaffer, "Egr1 is a 3D Matrix–specific Mediator of Mechanosensitive Stem Cell Lineage Commitment," *Science Advances* 8 (2022): abm4646, https://doi.org/10.1126/sciadv.abm4646.

9. N. R. Richbourg, N. Irakoze, H. Kim, and S. R. Peyton, "Outlook and Opportunities for Engineered Environments of Breast Cancer Dormancy," *Science Advances* 10 (2024): adl0165, https://doi.org/10.1126/sciadv.adl0165.

10. A. N. Kundu, C. E. Dougan, S. Mahmoud, et al., "Tenascin-C Activation of Lung Fibroblasts in a 3D Synthetic Lung Extracellular Matrix Mimic," *Advanced Materials* 35 (2023): 2301493, https://doi.org/10.1002/adma.202301493.

11. L. E. Jansen, H. Kim, C. L. Hall, T. P. McCarthy, M. J. Lee, and S. R. Peyton, "A Poly(ethylene glycol) Three-dimensional Bone Marrow Hydrogel," *Biomaterials* 280 (2022): 121270, https://doi.org/10.1016/j.biomaterials.2021.121270.

12. S. Galarza, A. J. Crosby, C. Pak, and S. R. Peyton, "Control of Astrocyte Quiescence and Activation in a Synthetic Brain Hydrogel," *Advanced Healthcare Materials* 9 (2020): 1901419, https://doi.org/10.1002/adhm.201901419.

13. N. J. Darling, Y.-S. Hung, S. Sharma, and T. Segura, "Controlling the Kinetics of Thiol-maleimide Michael-type Addition Gelation Kinetics for the Generation of Homogenous Poly(ethylene glycol) Hydrogels," *Biomaterials* 101 (2016): 199–206, https://doi.org/10.1016/j.biomaterials.2016.05.053.

14. L. E. Jansen, L. J. Negrón-Piñeiro, S. Galarza, and S. R. Peyton, "Control of Thiol-maleimide Reaction Kinetics in PEG Hydrogel Networks," *Acta Biomaterialia* 70 (2018): 120–128, https://doi.org/10.1016/j.actbio.2018.01.043.

15. C. Wang and C. Qi, "Mechanistic Insights Into N- or P-Centered Nucleophile Promoted Thiol–vinylsulfone Michael Addition," *Tetrahedron* 69 (2013): 5348–5354, https://doi.org/10.1016/j.tet.2013.04.123.

16. P. Yang, G. Boer, F. Snow, et al., "Test and Tune: Evaluating, Adjusting and Optimising the Stiffness of Hydrogels to Influence Cell Fate," *Chemical Engineering Journal* 505 (2025): 159295, https://doi.org/10.1016/j.cej.2025.159295.

17. C. J. F. Reyes, S. Pradhan, and J. H. Slater, "The Influence of Ligand Density and Degradability on Hydrogel Induced Breast Cancer Dormancy and Reactivation," *Advanced Healthcare Materials* 10 (2021): 2002227, https://doi.org/10.1002/adhm.202002227.

18. S. Q. Liu, Q. Tian, L. Wang, et al., "Injectable Biodegradable Poly(ethylene glycol)/RGD Peptide Hybrid Hydrogels for in Vitro Chondrogenesis of Human Mesenchymal Stem Cells," *Macromolecular Rapid Communications* 31 (2010): 1148–1154, https://doi.org/10.1002/marc.200900818.

19. N. Zhao, M. R. Battig, M. Xu, X. Wang, N. Xiong, and Y. Wang, "Development of a Dual-Functional Hydrogel Using RGD and Anti-VEGF Aptamer," *Macromolecular Bioscience* 17 (2017): 1700201, https://doi.org/10.1002/mabi.201700201.

20. J. S. Gnecco, A. Brown, K. Buttrey, et al., "Organoid co-culture Model of the human Endometrium in a Fully Synthetic Extracellular Matrix Enables the Study of Epithelial-stromal Crosstalk," *Med* 4 (2023): 554, https://doi.org/10.1016/j.medj.2023.07.004.

21. A. Yao, W. Huang, and H. Rubin, "Growth in High Serum Concentrations Leads to Rapid Deadaptation of Cells Previously Adapted to Growth in an Extremely Low Concentration of Serum," *Proceedings of the National Academy of Sciences* 88 (1991): 9422–9425, https://doi.org/10.1073/pnas.88.21.9422.

22. K. Wolf, M. te Lindert, M. Krause, et al., "Physical Limits of Cell Migration: Control by ECM Space and Nuclear Deformation and Tuning by Proteolysis and Traction Force," *Journal of Cell Biology* 201 (2013): 1069–1084, https://doi.org/10.1083/jcb.201210152.

23. K. A. Kyburz and K. S. Anseth, "Three-dimensional hMSC Motility Within Peptide-functionalized PEG-based Hydrogels of Varying Adhe-

sivity and Crosslinking Density," *Acta Biomaterialia* 9 (2013): 6381–6392, https://doi.org/10.1016/j.actbio.2013.01.026.

24. N. R. Richbourg and N. A. Peppas, "Solute Diffusion and Partitioning in Multi-arm Poly(ethylene glycol) Hydrogels," *Journal of Materials Chemistry B* 11 (2023): 377–388, https://doi.org/10.1039/D2TB02004A.

25. N. R. Richbourg, A. Ravikumar, and N. A. Peppas, "Solute Transport Dependence on 3D Geometry of Hydrogel Networks," *Macromolecular Chemistry and Physics* 222 (2021): 2100138, https://doi.org/10.1002/macp.202100138.

26. N. R. Richbourg and N. A. Peppas, "High-Throughput FRAP Analysis of Solute Diffusion in Hydrogels," *Macromolecules* 54 (2021): 10477–10486, https://doi.org/10.1021/acs.macromol.1c01752.

27. L. E. Barney, C. L. Hall, A. D. Schwartz, et al., "Tumor Cell–organized Fibronectin Maintenance of a Dormant Breast Cancer Population," *Science Advances* 6 (2020): aaz4157, https://doi.org/10.1126/sciadv.aaz4157.

28. O. Chaudhuri, J. Cooper-White, P. A. Janmey, D. J. Mooney, and V. B. Shenoy, "Effects of Extracellular Matrix Viscoelasticity on Cellular Behaviour," *Nature* 584 (2020): 535–546, https://doi.org/10.1038/s41586-020-2612-2.

29. R. Rizzo, N. Petelinšek, A. Bonato, and M. Zenobi-Wong, "From Free-Radical to Radical-Free: A Paradigm Shift in Light-Mediated Biofabrication," *Advanced Science* 10 (2023): 2205302, https://doi.org/10.1002/advs.202205302.

30. C. G. Williams, A. N. Malik, T. K. Kim, P. N. Manson, and J. H. Elisseeff, "Variable Cytocompatibility of Six Cell Lines With Photoinitiators Used for Polymerizing Hydrogels and Cell Encapsulation," *Biomaterials* 26 (2005): 1211–1218, https://doi.org/10.1016/j.biomaterials.2004.04.024.

31. E. R. Ruskowitz and C. A. DeForest, "Proteome-wide Analysis of Cellular Response to Ultraviolet Light for Biomaterial Synthesis and Modification," *ACS Biomaterials Science & Engineering* 5 (2019): 2111–2116, https://doi.org/10.1021/acsbiomaterials.9b00177.

32. B. D. Fairbanks, M. P. Schwartz, A. E. Halevi, C. R. Nuttelman, C. N. Bowman, and K. S. Anseth, "A Versatile Synthetic Extracellular Matrix Mimic via Thiol-Norbornene Photopolymerization," *Advanced Materials* 21 (2009): 5005–5010, https://doi.org/10.1002/adma.200901808.

33. J. I. Paez, A. Farrukh, R. Valbuena-Mendoza, M. K. Włodarczyk-Biegun, and A. del Campo, "Thiol-Methylsulfone-Based Hydrogels for 3D Cell Encapsulation," *ACS Applied Materials & Interfaces* 12 (2020): 8062–8072, https://doi.org/10.1021/acsami.0c00709.

34. E. A. Phelps, N. O. Enemchukwu, V. F. Fiore, et al., "Maleimide Cross-Linked Bioactive PEG Hydrogel Exhibits Improved Reaction Kinetics and Cross-Linking for Cell Encapsulation and In Situ Delivery," *Advanced Materials* 24 (2012): 64–70, https://doi.org/10.1002/adma.201103574.

35. M. P. Lutolf and J. A. Hubbell, "Synthesis and Physicochemical Characterization of End-Linked Poly(ethylene glycol)-co-peptide Hydrogels Formed by Michael-Type Addition," *Biomacromolecules* 4 (2003): 713–722, https://doi.org/10.1021/bm025744e.

36. A. C. Daly, L. Riley, T. Segura, and J. A. Burdick, "Hydrogel Microparticles for Biomedical Applications," *Nature Reviews Materials* 5 (2020): 20–43, https://doi.org/10.1038/s41578-019-0148-6.

37. V. Hernandez-Gordillo, T. Kassis, A. Lampejo, et al., "Fully Synthetic Matrices for in Vitro Culture of Primary human Intestinal Enteroids and Endometrial Organoids," *Biomaterials* 254 (2020): 120125, https://doi.org/10.1016/j.biomaterials.2020.120125.

38. G. J. Rodriguez-Rivera, M. Green, V. Shah, K. Leyendecker, and E. Cosgriff-Hernandez, "A User's Guide to Degradation Testing of Polyethylene Glycol-based Hydrogels: From in Vitro to in Vivo Studies," *Journal of Biomedical Materials Research Part A* (2023), https://doi.org/10.1002/jbm.a.37609.

39. T. S. Hebner, B. E. Kirkpatrick, B. D. Fairbanks, C. N. Bowman, K. S. Anseth, and D. S. W. Benoit, "Radical-Mediated Degradation of Thiol–Maleimide Hydrogels," *Advanced Science* 11 (2024): 2402191, https://doi.org/10.1002/advs.202402191.

40. Y. Wu, S. J. Rozans, A. S. Moghaddam, and E. T. Pashuck, "Using High-Throughput Screening to Identify Crosslinking Peptides That Control Cell-Mediated Matrix Degradation," *Advanced Healthcare Materials* 14 (2025): 01932, https://doi.org/10.1002/adhm.202501932.

41. A. Brown, H. He, E. Trumper, J. Valdez, P. Hammond, and L. G. Griffith, "Engineering PEG-based Hydrogels to Foster Efficient Endothelial Network Formation in Free-swelling and Confined Microenvironments," *Biomaterials* 243 (2020): 119921, https://doi.org/10.1016/j.biomaterials.2020.119921.

42. A. Franco, B. Van Durme, S. Van Vlierberghe, and C. Dupont-Gillain, "Misleading Pore Size Measurements in Gelatin and Alginate Hydrogels Revealed by Confocal Microscopy," *Tissue Engineering Part C: Methods* 30 (2024): 307–313, https://doi.org/10.1089/ten.tec.2024.0117.

43. L. Fischer and I. Thievessen, *Cell Viability Assays: Methods and Protocols* (Springer US, 2023), 371–385.

44. G. P. Raeber, M. P. Lutolf, and J. A. Hubbell, "Molecularly Engineered PEG Hydrogels: A Novel Model System for Proteolytically Mediated Cell Migration," *Biophysical Journal* 89 (2005): 1374–1388, https://doi.org/10.1529/biophysj.104.050682.

45. L. A. Sawicki, E. M. Ovadia, L. Pradhan, et al., "Tunable Synthetic Extracellular Matrices to Investigate Breast Cancer Response to Biophysical and Biochemical Cues," *APL Bioengineering* 3 (2019): 016101, https://doi.org/10.1063/1.5064596.

46. F. Chambon and H. H. Winter, "Linear Viscoelasticity at the Gel Point of a Crosslinking PDMS With Imbalanced Stoichiometry," *Journal of Rheology* 31 (1987): 683–697, https://doi.org/10.1122/1.549955.

47. H. H. Winter and F. Chambon, "Analysis of Linear Viscoelasticity of a Crosslinking Polymer at the Gel Point," *Journal of Rheology* 30 (1986): 367–382, https://doi.org/10.1122/1.549853.

48. L. Poh, E. Narimissa, and M. H. Wagner, "Interactive Shear and Extensional Rheology—25 years of IRIS Software," *Rheologica Acta* 61 (2022): 259–269, https://doi.org/10.1007/s00397-022-01331-6.

49. E. J. De Souza, L. Gao, T. J. McCarthy, E. Arzt, and A. J. Crosby, "Effect of Contact Angle Hysteresis on the Measurement of Capillary Forces," *Langmuir* 24 (2008): 1391–1396, https://doi.org/10.1021/la702188t.

50. N. R. Richbourg, M. K. Rausch, and N. A. Peppas, "Cross-evaluation of Stiffness Measurement Methods for Hydrogels," *Polymer* 258 (2022): 125316, https://doi.org/10.1016/j.polymer.2022.125316.

51. A. J. Dominijanni, M. Devarasetty, S. D. Forsythe, K. I. Votanopoulos, and S. Soker, "Cell Viability Assays in Three-Dimensional Hydrogels: A Comparative Study of Accuracy," *Tissue Engineering Part C: Methods* 27 (2021): 401–410, https://doi.org/10.1089/ten.tec.2021.0060.

Supporting Information

Additional supporting information can be found online in the Supporting Information section.

Supporting File: adma72553-sup-0001-SuppMat.docx.